Journal of Alloys and Compounds 509 (2011) 3515–3521

Contents lists available at ScienceDirect

Journal of Alloys and Compounds

journal homepage: www.elsevier.com/locate/jallcom

The relationship between $(Mg,Zn)_3RE$ phase and 14H-LPSO phase in Mg–Gd–Y–Zn–Zr alloys solidified at different cooling rates

S. Zhang[a,b], G.Y. Yuan[a,b,*], C. Lu[a,b], W.J. Ding[a,b]

[a] National Engineering Research Center of Light Alloy Net Forming, Shanghai Jiao Tong University, 800 Dongchuan Road, Shanghai 200240, PR China
[b] State Key Laboratory of Metal Matrix Composite, Shanghai Jiao Tong University, 800 Dongchuan Road, Shanghai 200240, PR China

ARTICLE INFO

Article history:
Received 8 December 2010
Accepted 16 December 2010
Available online 24 December 2010

Keywords:
Mg–Gd–Y–Zn alloys
Long period stacking ordered structure
Cooling rate
Orientation relationship

ABSTRACT

Mg–10Gd–3Y–1.8Zn–0.5Zr (wt.%) (GWZ1032K) alloys are prepared by permanent mold casting at cooling rate of 5 K/s, or further prepared by melt spinning at cooling rate of 10^4 K/s, or by slow solidification at different cooling rates (0.5 K/s, 0.1 K/s, 0.01 K/s and 0.005 K/s). $(Mg,Zn)_3RE$ phase and 14H-LPSO structure in alloys under different conditions are measured by XRD and observed under electron microscope. It shows there is no LPSO structure in the alloy prepared by melt spinning at cooling rate of 10^4 K/s. In the alloy prepared by permanent mold casting at cooling rate of 5 K/s, fine lamellar 14H-LPSO structure appears in the matrix nearby grain boundaries. With the cooling rates slowing down from 0.5 K/s to 0.005 K/s, $(Mg,Zn)_3RE$ phase is gradually replaced by 14H-LPSO phase at grain boundaries, and lamellar 14H-LPSO structure also propagates in α-Mg matrix. Both $(Mg,Zn)_3RE$ phase and 14H-LPSO phase are present at grain boundaries in the alloys solidified at cooling rates of 0.5 K/s and 0.1 K/s. When the cooling rate is very slow (0.005 K/s), lamellar 14H-LPSO structure penetrates throughout the matrix grain. It suggests the cooling rate is an important factor for the formation of 14H-LPSO structure in as-cast GWZ1032K alloys. The orientation relationship between $(Mg,Zn)_3RE$ phase and 14H-LPSO phase is determined by the composite SAED patterns, which is expressed as $(1\,1\,0)_{(Mg,Zn)3RE}//(0\,0\,1\,4)_{14H\text{-}LPSO\ phase}$, $[\bar{3}\,3\,2]_{(Mg,Zn)3RE}//[1\,1\,0]_{14H\text{-}LPSO\ phase}$ and $[\bar{1}\,1\,2]_{(Mg,Zn)3RE}//[2\,1\,0]_{14H\text{-}LPSO\ phase}$.

1. Introduction

Recently, there has been increasing interest in the use of Mg alloys for applications in automobiles and aircrafts, due to their light weight and good mechanical properties. As new light structural materials, it is projected that the age-hardenable Mg–Gd–Y–Zr alloys represent super high strength and excellent creep resistance at both ambient and elevated temperatures [1–4]. However, their plasticity is very poor and thus limits their application, because the high content of rare earth (RE) is up to 10 wt.% or so. A number of cast Mg alloys containing small amount of Zn have been investigated recently [5–17]. These investigations have shown that Zn can be used to improve mechanical properties due to the formation of long period stacking ordered (LPSO) structure. A previous study reported the rapidly solidified powder metallurgy $Mg_{97}Zn_1Y_2$ alloys [5], with LPSO structure, performed remarkable high strength (>600 MPa) and high ductility. The main reason for the excellent mechanical properties of these alloys is that the existence of LPSO structure improves the hardness and strength of Mg alloys [6,7].

In Mg–Gd–Zn and Mg–Gd–Y–Zn alloys prepared by permanent mold casting, LPSO structure is precipitated as 14H from the matrix upon annealing [8–10]. Yamasaki et al. [9] found that the microstructure of as-cast Mg–Gd–Zn alloy was composed of α-Mg matrix and eutectic compounds at grain boundaries, acknowledged as DO_3-type $(Mg,Zn)_3Gd$ phase and α-Mg. Wu et al. [11,12] observed preciously little 14H-LPSO structured lamellae in α-Mg matrix close to grain boundaries in as-cast Mg–Gd–Zn alloy. This work also pointed out that in Mg–Gd–Zn alloy heat-treated at 773 K, 14H-LPSO phase was transformed from eutectic phase and the transformation mechanism is considered as spinodal decomposition.

With respect to the fact that LPSO structure has been observed in Mg–Gd–Y–Zn alloys [13–17], the nature of LPSO structure is further investigated in this study. We observed the characteristic morphologies of 14H-LPSO structure in Mg–Gd–Y–Zn alloys solidified at different cooling rates. The orientation relationship between $(Mg,Zn)_3RE$ phase and 14H-LPSO phase has been demonstrated.

2. Experimental procedure

For the present investigation, Mg–10Gd–3Y–1.8Zn–0.4Zr (wt.%, refer to GWZ1032K hereafter) was prepared in an electric resistance furnace under a mixed

* Corresponding author at: National Engineering Research Center of Light Alloy Net Forming, Shanghai Jiao Tong University, 800 Dongchuan Road, Shanghai 200240, PR China. Tel.: +86 21 34203051; fax: +86 21 34202794.
E-mail address: gyyuan@sjtu.edu.cn (G.Y. Yuan).

0925-8388/$ – see front matter © 2010 Elsevier B.V. All rights reserved.
doi:10.1016/j.jallcom.2010.12.136

Table 1
GWZ1032K alloys solidified at different cooling rates.

Alloy	Solidification condition
A (rapidly solidified alloy)	Melt-spinning at a wheel speed of 10 m/s, about cooling rate of 10^4 K/s
B (the master alloy)	Permanent mold casting at the cooling rate of 5 K/s
C (slowly solidified alloy)	Cooling rate of 0.5 K/s from 923 K to 723 K, followed by quenching in cold water
D (slowly solidified alloy)	Cooling rate of 0.1 K/s from 923 K to 723 K, followed by quenching in cold water
E (slowly solidified alloy)	Cooling rate of 0.01 K/s from 923 K to 723 K, followed by quenching in cold water
F (slowly solidified alloy)	Cooling rate of 0.005 K/s from 923 K to 723 K, followed by quenching in cold water

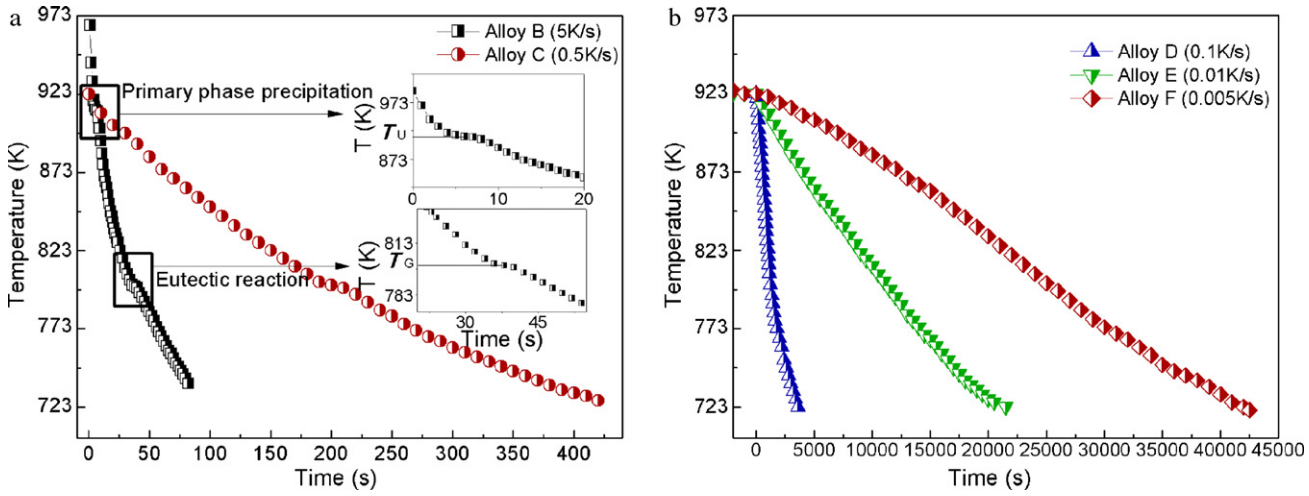

Fig. 1. (a) Cooling curves of Alloys B and C at the rates of 5 K/s and 0.5 K/s, respectively. (b) Cooling curves of Alloys D, E and F at the rates of 0.1 K/s, 0.01 K/s and 0.005 K/s, respectively.

atmosphere of CO_2 and SF_6 with 100:1 ratio. The raw materials were pure Mg and Zn (>99.95%), and Mg–25 wt.% Gd, Mg–25 wt.% Y and Mg–30 wt.% Zr. The alloy ingots were cast in a permanent mold and cooled in air.

Six GWZ1032K specimens are arranged in Table 1 according to the cooling rates from high to low. Alloy B was prepared with permanent mold casting at the cooling rate of 5 K/s and used as the master alloy. Alloys A, C, D, E and F were obtained from the master alloy with the specific treatment. Alloy A was produced from the master alloy, re-melted using induction melting and then prepared by melt spinning method at the roller surface velocity of 10 m/s in purified melt atmosphere. The cooling rate of the as-spun ribbons for Alloy A was calculated 10^4 K/s according to the method published in previous study [18]. The four specimens of slow solidification were fabricated as follows. The master alloys were protected by cover agents and placed in the graphite crucible of the heat treatment furnace with sulfurous iron ore. Alloys were heated at 923 K for 30 min for complete melt and solute homogenization. After that, the temperature dropped off from 923 K to 723 K at four different cooling rates. After reaching 723 K, the specimens were taken out and quenched in cold water. The cooling rates for Alloys C, D, E and F were calculated in accordance with the cooling curves and expressed as 0.5 K/s, 0.1 K/s, 0.01 K/s and 0.005 K/s, respectively. At the same time, the temperature within the furnace was controlled by the temperature controller. In order to measure the actual cooling rates of the alloys, a thermocouple was inserted into the graphite crucible to achieve the temperature of the melting alloys. The cooling curves of the alloys were acquired by using data collection module and are presented in Fig. 1.

To investigate the microstructure, all materials were grinded, polished and etched. Microstructures were investigated using a LEO1450 scanning electron microscope (SEM) including an energy-dispersive X-ray analysis (EDS) to determine the local chemical compositions. Transmission electron microscopy (TEM) investigations were employed on thin foil samples of the different GWZ1032K alloys. The foils were prepared by electropolishing in a twin jet system using a solution of 4% $HClO_4$ and 96% methanol at 253 K and a voltage of 50 V. The TEM examinations were carried out using a JEOL-2010 instrument operating at 200 kV. For the phase analysis, X-ray diffraction (XRD) measurements were also performed using a Bruker D8 Advance (Bruker AXS, Karlsruhe, Germany).

3. Results

The XRD measurements shown in Fig. 2 could prove the presence of α-Mg phase, $(Mg,Zn)_3RE$ phase or 14H-LPSO phase in the diffraction patterns for six alloys. The typical α-Mg peaks are present in all alloys. Only α-Mg phase (marked with hollow triangles) is recognized from the pattern of Alloy A. Both α-Mg and $(Mg,Zn)_3RE$ phase (marked with hollow circles) are observed in Alloy B, this finding is also in agreement with the investigations of Yamasaki et al. [9]. Apart from α-Mg and $(Mg,Zn)_3RE$ phase, an additional peaks of 14H-LPSO phase (marked with hollow rhombuses) are identified from the patterns of Alloys C and D. However, only α-Mg and 14H-LPSO phase are recognized from the patterns of Alloys E and F.

The microstructure revealed by TEM is shown for Alloy A in Fig. 3. Fig. 3a shows a typical TEM bright-field (BF) image of the microstructure of Alloy A. The dendrite within area A in Fig. 3a is α-Mg phase, confirmed by using selected area electron diffraction (SAED) patterns with the electron beam parallel to the [0 1 $\bar{1}$ 1]

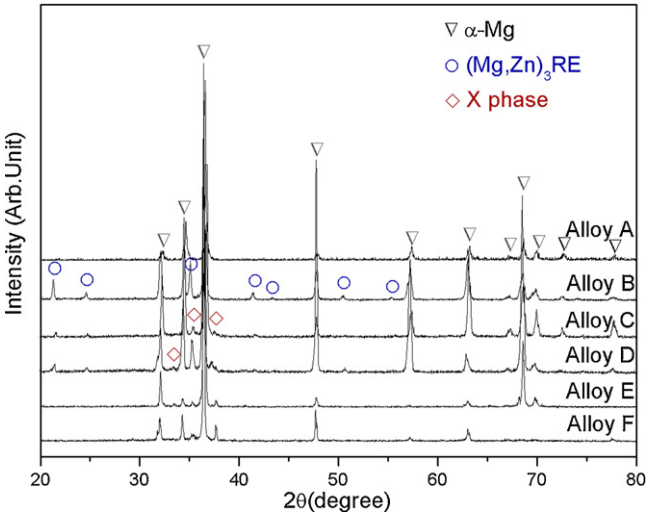

Fig. 2. The XRD patterns of Alloys A, B, C, D, E and F.

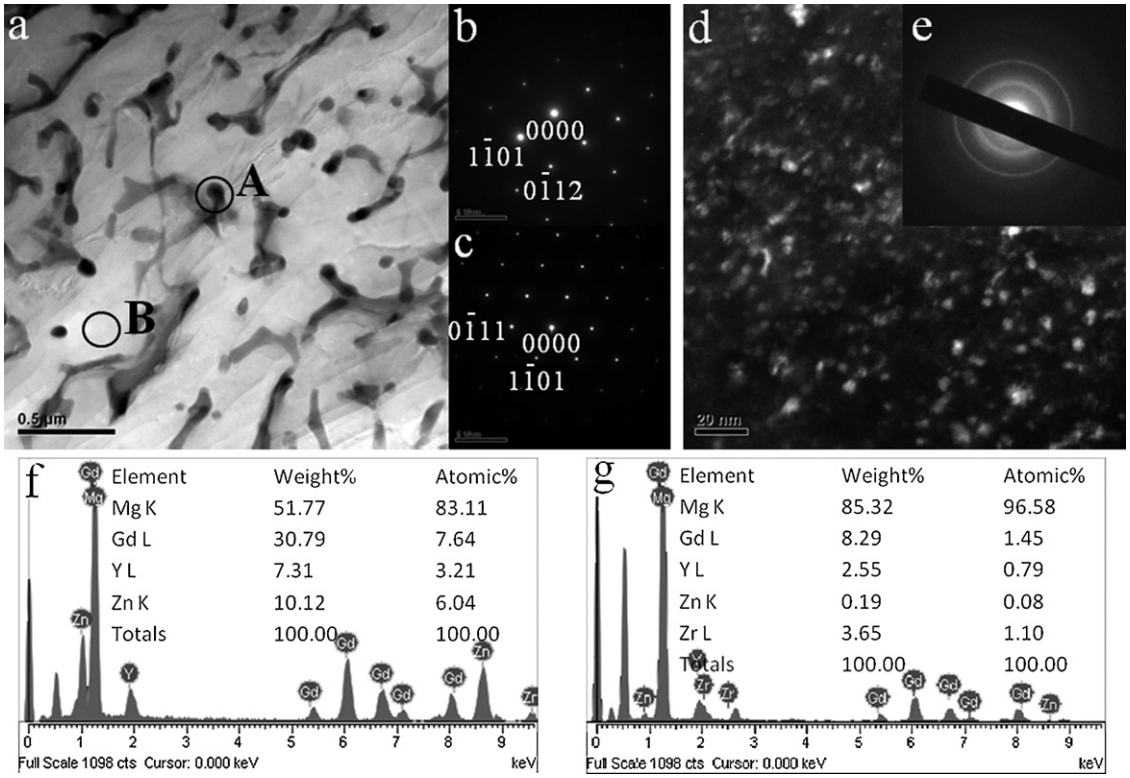

Fig. 3. Microstructure of Alloy A: (a) TEM BF image, (b, c) SAED patterns of the dendrite in area A ($B = [0\,1\,\bar{1}\,1]_{\alpha\text{-Mg}}$ and $[1\,\bar{2}\,1\,\bar{3}]_{\alpha\text{-Mg}}$), (d) TEM dark-field image of area B, (e) SAED pattern of area B.

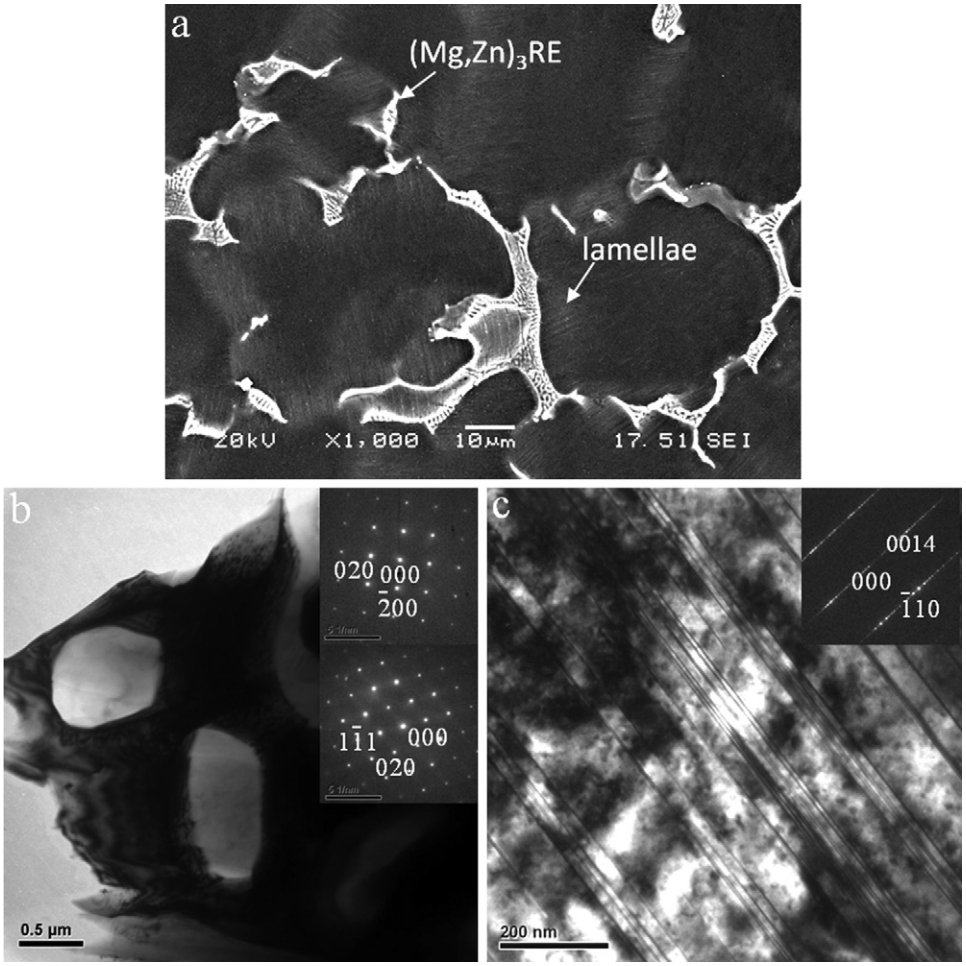

Fig. 4. Microstructure of Alloy B: (a) SEM image, (b) TEM BF image and SAED patterns ($B = [001]_{(Mg,Zn)3RE}$ and $[011]_{(Mg,Zn)3RE}$) of eutectic phase, (c) TEM BF image and SAED pattern ($B = [110]_{\alpha\text{-Mg}}$) of lamellar 14H-LPSO structure.

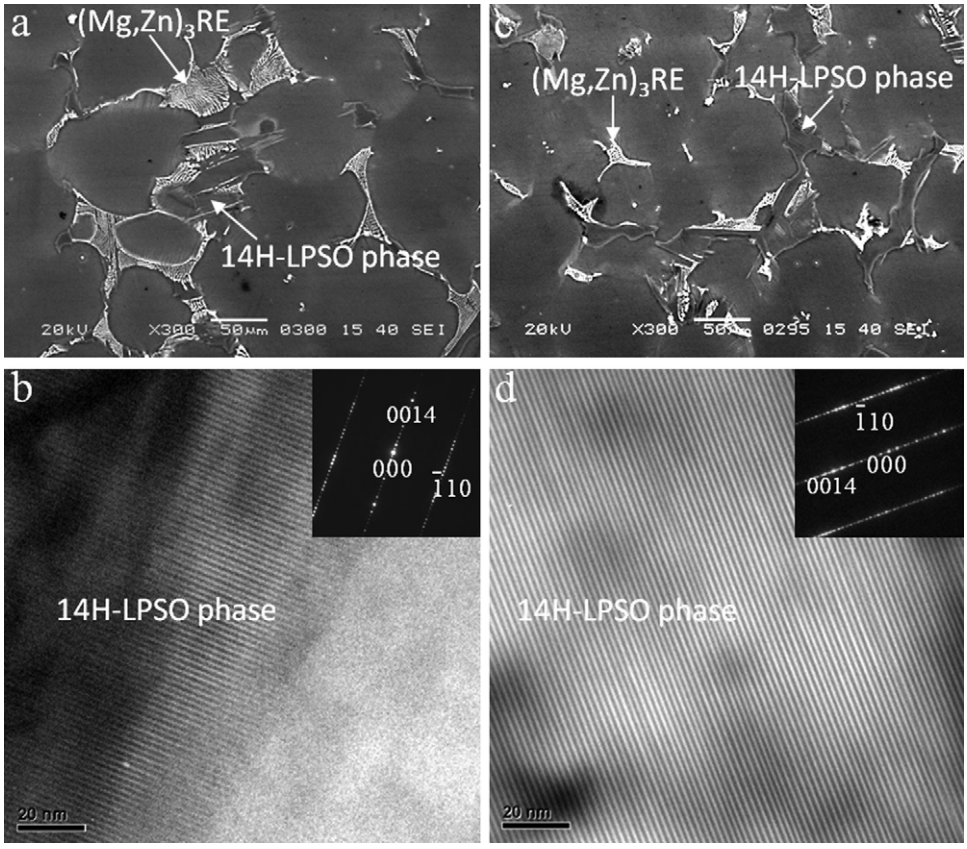

Fig. 5. Microstructure of Alloys C and D. SEM image (a), TEM BF image (b) and SAED pattern ($B=[110]_{\alpha\text{-Mg}}$) of Alloy C. SEM image (c), TEM BF image (d) and SAED pattern ($B=[110]_{\alpha\text{-Mg}}$) of Alloy D.

and $[1\,\bar{2}\,1\,\bar{3}]$ zones respectively (Fig. 3b and c). A dark-field electron micrograph and SAED pattern of area B note that the matrix is composed of α-Mg nanoscale particles (Fig. 3d and e). α-Mg nanoscale particle has a size smaller than 10 nm and appears an ellipsoidal shape. There is no LPSO structure found in Alloy A. The comparison of the EDS spectrums between the dendrite (Fig. 3f) and nanoscale particles (Fig. 3g) illustrates that the content of Gd, Y and Zn atoms in the dendrite is significantly more than that in nanoscale particles. This result suggests the dendrite within area A is α-Mg supersaturated solid solution.

Fig. 4 shows the microstructure of Alloy B casted by permanent metal mold. As shown in Fig. 4a, eutectic compounds are discontinuously located at grain boundaries. Fine lamellae formed on specific habit plane of α-Mg grains are close to grain boundaries. Typical TEM BF images and corresponding SAED patterns for eutectic phase and fine lamellae are shown in Fig. 4b and c respectively. The SAED pattern of eutectic phase ($B=[0\,0\,1]$ and $[0\,1\,1]$ respectively) indicates that it has a cubic structure ($a=0.7283$ nm) (Fig. 4b). The EDS spectrum indicates eutectic phase has an average composition of 65 ± 3Mg–21.5 ± 2Gd–3.5 ± 1Y–6 ± 10Zn (at.%), i.e. $(Mg,Zn)_3(Gd,Y)_1$. The XRD measurement of eutectic phase (Fig. 2) is also coincident with Mg_3Gd phase (DO_3, $a=0.7324$ nm [19]). In this study, eutectic phase is formulated as DO_3-type $(Mg,Zn)_3RE$ phase, whereas the second phase in as-cast GW103K alloy without Zn content is identified as $Mg_{24}(Gd,Y)$ by our previous work [4]. In Fig. 4c, the SAED pattern of fine lamellae in the matrix ($B=[1\,1\,0]_{\alpha\text{-Mg}}$) shows it has a 14H-type LPSO structure ($a=0.3370$ nm, $c=3.5789$ nm), with the evidence of 13 extra spots spacing equally between the central spot and the $(0\,0\,2)_{Mg}$ spot.

Fig. 5 presents the microstructure of Alloys C and D solidified slowly at the cooling rates of 0.5 K/s and 0.1 K/s, respectively. Besides $(Mg,Zn)_3RE$ phase, 14H-LPSO phase appears at the grain boundaries both in Alloy C (Fig. 5a) and Alloy D (Fig. 5b). Typical TEM BF image and SAED pattern ($B=[1\,1\,0]_{14\text{H-LPSO phase}}$) of 14H-LPSO phase are shown in Fig. 5c and d. The SAED pattern indicates that there is it also has a 14H-LPSO structure ($a=0.3375$ nm, $c=3.5810$ nm). The EDS spectrum indicates 14H-LPSO phase has an average composition of 88 ± 3Mg–4.5 ± 2Gd–1.5 ± 1Y–6 ± 2Zn (at.%), i.e. $Mg_{12}(Gd,Y)_1Zn_1$. The XRD pattern of 14H-LPSO phase (Fig. 2) is also in agreement with $Mg_{12}YZn$ phase in Mg–Y–Zn alloys [20].

Fig. 6 shows a magnified SEM image of $(Mg,Zn)_3RE$ phase, 14H-LPSO phase and fine lamellae in Alloy D. $(Mg,Zn)_3RE$ phase and 14H-LPSO phase are connective with each other at grain

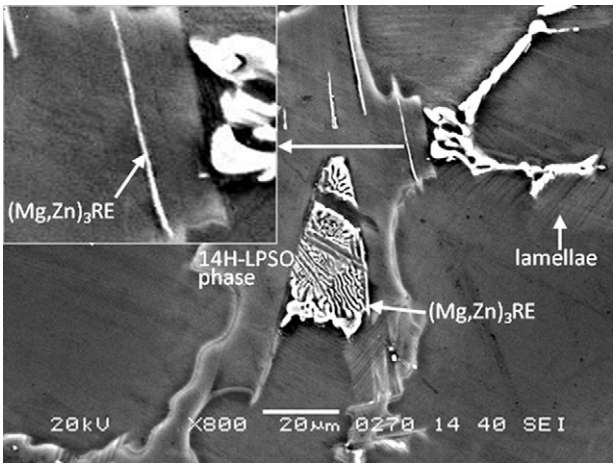

Fig. 6. Magnified SEM image of Alloy D.

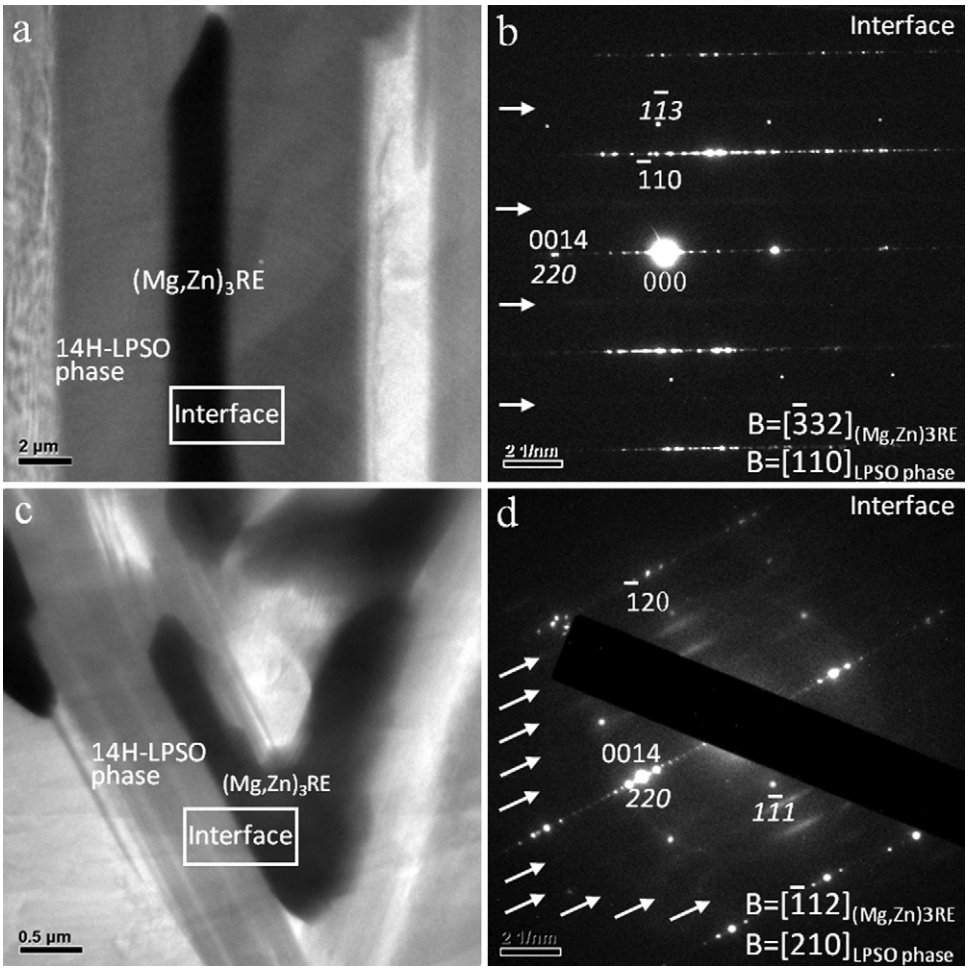

Fig. 7. $(Mg,Zn)_3RE$ phase and 14H-LPSO structure in Alloy D. TEM BF image (a) and SAED pattern (b) obtained from the interface between needle-shaped $(Mg,Zn)_3RE$ phase and 14H-LPSO phase. TEM BF image (c) and SAED pattern (d) obtained from the interface between eutectic $(Mg,Zn)_3RE$ phase and 14H-LPSO phase. The electron beam is parallel to $[\bar{3}\,3\,2]_{(Mg,Zn)3RE}$ and $[1\,1\,0]_{14H\text{-}LPSO\ phase}$ (a, b), $[\bar{1}\,1\,2]_{(Mg,Zn)3RE}$ and $[2\bar{1}0]_{14H\text{-}LPSO\ phase}$ (c, d). Weak streaks are indicated by white arrows (b, d).

boundaries. The needle-shaped $(Mg,Zn)_3RE$ phase is identified in 14H-LPSO phase and the eutectic $(Mg,Zn)_3RE$ phase connects tightly with 14H-LPSO phase. Both the needle-shaped and eutectic $(Mg,Zn)_3RE$ phases have a specific habit plane with 14H-LPSO phase.

Fig. 7 shows TEM BF images and corresponding SAED patterns of $(Mg,Zn)_3RE$ phase and 14H-LPSO phase at grain boundaries. The needle-shaped $(Mg,Zn)_3RE$ phase is surrounded by 14H-LPSO phase (Fig. 7a). The corresponding composite SAED pattern of $(Mg,Zn)_3RE$ phase and 14H-LPSO phase obtained from their interface (Fig. 7b) indicates $(1\,1\,0)_{(Mg,Zn)3RE}//(0\,0\,1\,4)_{14H\text{-}LPSO\ phase}$ and $[\bar{3}\,3\,2]_{(Mg,Zn)3RE}//[1\,1\,0]_{14H\text{-}LPSO\ phase}$. Fig. 7c shows the eutectic $(Mg,Zn)_3RE$ phase links with 14H-LPSO phase. The corresponding $(Mg,Zn)_3RE$ phase/14H-LPSO phase SAED pattern (Fig. 7d) indicates $(1\,1\,0)_{(Mg,Zn)3RE}//(0\,0\,1\,4)_{14H\text{-}LPSO\ phase}$ and $[\bar{1}\,1\,2]_{(Mg,Zn)3RE}//[2\,1\,0]_{14H\text{-}LPSO\ phase}$. In Fig. 7b, parallel weak streaks arise along the direction of $g(0\,0\,1)_{14H\text{-}LPSO\ phase}$ and through the $\pm1/2\{\bar{1}\,1\,0\}_{14H-LPSO\ phase}$ positions. In Fig. 7d, parallel weak streaks arise along the direction of $g(0\,0\,1)_{14H\text{-}LPSO\ phase}$ and through the $\pm1/6\{\bar{1}\,2\,0\}_{14H-LPSO\ phase}$, $\pm2/6\{\bar{1}\,2\,0\}_{14H-LPSO\ phase}$, $\pm3/6\{\bar{1}\,2\,0\}_{14H-LPSO\ phase\ 14H\text{-}LPSO\ phase}$, $\pm4/6\{\bar{1}\,2\,0\}_{14H-LPSO\ phase}$ or $\pm5/6\{\bar{1}\,2\,0\}_{14H-LPSO\ phase}$ positions.

Two kinds of 14H-LPSO structures were observed in Alloys E and F, they are 14H-LPSO phase and lamellar 14H-LPSO structure (Fig. 8). 14H-LPSO phase is observed at grain boundaries. Lamellar 14H-LPSO structure is formed on specific habit plane of α-Mg grains. In contrast to fine lamellae in Alloy B, lamellar 14H-LPSO structure in Alloys E and F is more prominent. In Alloy E, lamellar 14H-LPSO structure arranges nearby grain boundaries but does not penetrate throughout the grains (Fig. 8b). In Alloy F, the volume fraction of lamellar 14H-LPSO structure is much higher and every grain is penetrated by these lamellae (Fig. 8d).

4. Discussion

There are two categories of 14H-LPSO structures emerging in as-cast GWZ1032K alloys during solidification, known as 14H-LPSO phase and lamellar 14H-LPSO structure. 14H-LPSO phase is as a second phase formed at grain boundaries. Lamellar 14H-LPSO structure is located in the α-Mg matrix, it is close to grain boundaries. The morphologies of two 14H-LPSO structures are changing dynamically under different solidification conditions.

In Alloy B casted by permanent metal mold, the solute segregation is prominent due to a relatively high cooling rate (5 K/s). RE and Zn atoms in Alloy B are segregated at grain boundaries to form $(Mg,Zn)_3RE$ phase by eutectic reaction, which is followed with the nucleation of α-Mg matrix. The degree of solute segregation declines with the cooling rate slowing down, thus the volume fraction of $(Mg,Zn)_3RE$ phase decreases and 14H-LPSO phase begins to form at grain boundaries. Ultimately, only 14H-LPSO phase exists at grain boundaries and $(Mg,Zn)_3RE$ phase disappears. In addition, the volume fraction of lamellar 14H-LPSO structure in the matrix

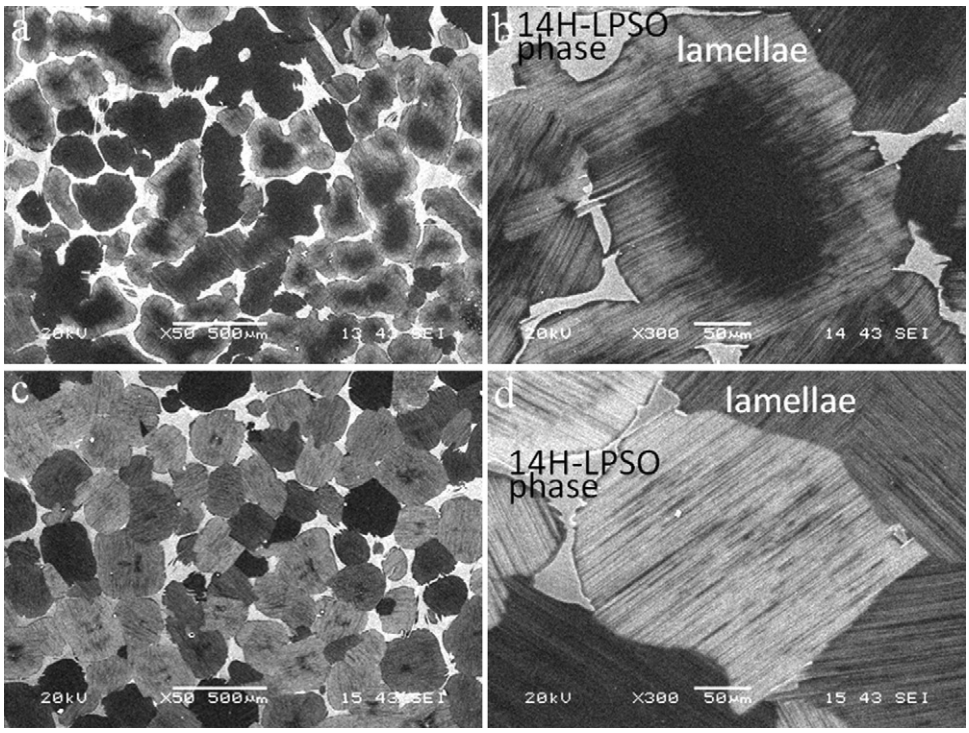

Fig. 8. SEM images show the microstructure of Alloy E (a, b) and Alloy F (c, d). In Alloy E, lamellar 14H-LPSO structure arranges nearby grain boundaries but does not penetrate throughout the grains. In Alloy F, the volume fraction of lamellar 14H-LPSO structure is much higher and the grains are totally filled with the lamellae.

increases with the cooling rate slowing down. The alloy cools down slowly so that RE and Zn atoms diffuse into the matrix, thus lamellar 14H-LPSO structure has enough time to nucleate and propagate. When the cooling rate is very slow, lamellar 14H-LPSO structure cross over the matrix grain as shown in Alloy F.

Datta et al. [21] reported that the energy of 14H-LPSO structure is fairly close to that of the hcp structure, indicating 14H-LPSO structure is a very stable structure. In this study, a stable 14H-LPSO structure tends to form in GWZ1032K alloy during solidification with the cooling rate slowing down. Take Alloy E (0.005 K/s) as an example, 14H-LPSO phase appears at grain boundaries and lamellar 14H-LPSO structure is significant in the matrix. The stacking sequence of 14H-LPSO structure in GWZ1032K alloy is identified as ABABCACACACBABA, which consists of two ABCA stacking sequence structural units [22–24]. It is well known that RE and Zn atoms are enriched in B and C layers in the ABCA structural unit [24]. The formation mechanism of 14H-LPSO structure is known as spinodal decomposition in Mg–Gd–Zn alloys [11,12]. The ordered arrangement of RE and Zn atoms in 14H-LPSO structure needs a driving force. But in Alloy A prepared by melt spinning, there was no enough driving force for the ordered arrangement of solute atoms (Gd, Y and Zn) because of a very high cooling rate. As a result, 14H-LPSO structure failed to form in Alloy A although the density of solute atoms kept a high level.

Ding et al. [25] reported the detailed microstructure evolution of Mg–Gd–Zn–Zr alloy heat-treated at high temperature was similar to that of GWZ1032K alloy treated at different cooling rates. They found that in the heat-treated Mg–Gd–Zn–Zr alloy at high temperature, DO_3-type $(Mg,Zn)_3RE$ phase at grain boundaries transformed into 14H-LPSO phase. Our study further investigated the mechanism of this transformation and the orientation relationship between $(Mg,Zn)_3RE$ phase and 14H-LPSO phase. Both $(Mg,Zn)_3RE$ phase and 14H-LPSO phase are observed at grain boundaries in GWZ1032K alloys at the rates of 0.5 K/s and 0.1 K/s. The orientation relationship between $(Mg,Zn)_3RE$ phase and 14H-LPSO phase was revealed by SAED patterns as $(1\,1\,0)_{(Mg,Zn)3RE}//(0\,0\,1\,4)_{14H\text{-}LPSO\ phase}$, $[\bar{3}\,3\,2]_{(Mg,Zn)3RE}//[1\,1\,0]_{14H\text{-}LPSO\ phase}$ and $[\bar{1}\,1\,2]_{(Mg,Zn)3RE}//[2\,1\,0]_{14H\text{-}LPSO\ phase}$. The finding of this orientation relationship is helpful to the researches on the transformation mechanism from $(Mg,Zn)_3RE$ phase to 14H-LPSO phase. We found that weak streaks are observed in SAED patterns obtained from the interface between $(Mg,Zn)_3RE$ phase and 14H-LPSO phase. Zhu pointed out that any disordered arrangement of RE and Zn atoms within the segregation layers would lead to the disappearance of streaks and intensity maxima in SAED patterns of LPSO structure in Mg–Y–Zn alloys [21]. It is considered that weak streaks maybe caused by the ordered arrangement of RE and Zn atoms and lattice distortion in the area near the interface.

Our study demonstrates the morphology and volume fraction of 14H-LPSO structure in GWZ1032K alloy are adjusted by the cooling rate. This finding indicates slow solidification, as well as hot extrusion [26] and rapidly solidified powder metallurgy [5], is one of methods to obtain Mg alloy with uniformly distributed LPSO structure.

5. Conclusion

We investigated the morphologies of 14H-LPSO structure in GWZ1032K alloys solidified at different cooling rates. The obtained conclusions are summarized as follows. We investigated the morphologies of 14H-LPSO structure in GWZ1032K alloys solidified at different cooling rates. The obtained conclusions are summarized as follows.

1 14H-LPSO structure, including 14H-LPSO phase and lamellar 14H-LPSO structure, is present in Alloy B (5 K/s), Alloy C (0.5 K/s), Alloy D (0.1 K/s), Alloy E (0.01 K/s) and Alloy F (0.005 K/s), but not present in Alloy A (10^4 K/s). It suggests that 14H-LPSO structure in as-cast GWZ1032K alloy increases with the cooling rate slowing down. When the cooling rate is very slow (0.005 K/s), lamellar 14H-LPSO structure propagates through the matrix grain.

2 The second phase at grain boundaries is variable in the as-cast GWZ1032K alloys at different cooling rates. Alloy B (5 K/s) has only $(Mg,Zn)_3RE$ phase. Both $(Mg,Zn)_3RE$ phase and 14H-LPSO phase are found in Alloy C (0.5 K/s) and Alloy D (0.1 K/s). There is only 14H-LPSO phase in Alloy E (0.01 K/s) and Alloy F (0.005 K/s).
3 The orientation relationship between $(Mg,Zn)_3RE$ phase and 14H-LPSO phase is determined by the composite SAED patterns to be $(1\,1\,0)_{(Mg,Zn)3RE}//(0\,0\,1\,4)_{14H\text{-}LPSO\ phase}$, $[\bar{3}\,3\,2]_{(Mg,Zn)3RE}//[1\,1\,0]_{14H-LPSO\ phase}$ and $[\bar{1}\,1\,2]_{(Mg,Zn)3RE}//[2\,1\,0]_{14H-LPSO\ phase}$. Weak streaks along the direction of $g(0\,0\,1)_{14H\text{-}LPSO\ phase}$ were also observed in the composite SAED patterns.

Acknowledgements

The authors acknowledge the financial support of the National Nature Science Foundation of China (No.: 50771063), and Science and Technology Commission of Shanghai Municipality (08JC1412200), and New-century Training Program Foundation for the Talents by the State Education Commission of China (WCET-07-0554). The authors want to express their gratitude to Prof. S.P. Chen and Prof. D.L. Lin for their valuable advice on the discussion of this paper. The authors thank the Instrumental Analysis Center of Shanghai Jiao Tong University for their technical support.

References

[1] L.L. Rokhin, Magnesium Alloys Containing Rare Earth Metals, Taylor and Francis, London, 2003, p. 1.
[2] S. Kamado, Y. Kojima, R. Ninomiya, K. Kubota, in: G.W. Lorimer (Ed.), Proceedings of the Third International Magnesium Conference, 1996, Institute of Materials, Machester, UK, 1997, p. 327.
[3] S.M. He, X.Q. Zeng, L.M. Peng, X. Gao, J.F. Nie, W.J. Ding, J. Alloy Compd. 427 (2007) 316.
[4] S.M. He, X.Q. Zeng, L.M. Peng, X. Gao, J.F. Nie, W.J. Ding, J. Alloy Compd. 421 (2006) 309.
[5] Y. Kawamura, K. Hayashi, A. Inoue, T. Masumoto, Mater. Trans. 42 (2001) 1172.
[6] T. Itoi, T. Seimiya, Y. Kawamura, M. Hirohashi, Mater. Sci. Forum. 419–422 (2003) 721.
[7] Y. Chino, M. Mabuchi, S. Hagiwara, H. Iwasaki, A. Yamamoto, H. Tsubakino, Scripta Mater. 51 (2004) 711.
[8] K. Liu, J.H. Zhang, G.H. Su, D.X. Tang, L.L. Rokhlin, F.M. Elkin, J. Meng, J. Alloy Compd. 481 (2009) 811.
[9] M. Yamasaki, M. Sasaki, M. Nishijima, K. Hiraga, Y. Kawamura, Acta Mater. 55 (2007) 6798.
[10] M. Yamasaki, T. Anan, S. Yoshimoto, Y. Kawamura, Scripta Mater. 53 (2005) 799.
[11] Y.J. Wu, X.Q. Zeng, D.L. Lin, L.M. Peng, W.J. Ding, J. Alloy Compd. 477 (2009) 193.
[12] Y.J. Wu, D.L. Lin, X.Q. Zeng, L.M. Peng, W.J. Ding, J. Mater. Sci. 44 (2009) 1607.
[13] Y. Gao, Q.D. Wang, J.H. Gu, Y. Zhao, Y. Tong, D.D. Yin, J. Alloy Compd. 477 (2009) 374.
[14] T. Honma, T. Ohkubo, S. Kamado, K. Hono, Acta Mater. 55 (2007) 4137.
[15] D.J. Li, X.Q. Zeng, J. Dong, C.Q. Zhai, W.J. Ding, J. Alloy Compd. 468 (2009) 164.
[16] X.B. Liu, R.S. Chen, E.H. Han, J. Alloy Compd. 465 (2008) 232.
[17] K. Yamada, Y. Okubo, S. Kamado, Y. Kojima, Adv. Mater. Res. 11–12 (2006) 417.
[18] X.H. Liu, W.L. Johnson, J. Appl. Phys. 78 (1995) 6514.
[19] V.P. Perminov, Powder Metall. Met. Ceram. 6 (1967) 409.
[20] E. Padezhnova, Russ. Metall. (Engl. Transl.) 1982 (1982) 185.
[21] A. Datta, U.V. Waghmare, U. Ramamurty, Acta Mater. 56 (2008) 2531.
[22] Y.M. Zhu, A.J. Morton, J.F. Nie, Acta Mater. 58 (2010) 2936.
[23] T. Itoi, T. Seimiya, Y. Kawamura, M. Hirohashi, Scripta Mater. 51 (2004) 107.
[24] Y.M. Zhu, M. Weyland, A.J. Morton, K. Oh-ishi, K. Honod, J.F. Nie, Scripta Mater. 60 (2009) 980.
[25] W.J. Ding, Y.J. Wu, L.M. Peng, X.Q. Zeng, G.Y. Yuan, D.L. Lin, J. Mater. Res. 24 (2009) 1842.
[26] K. Liu, J. Zhang, L.L. Rokhlin, F.M. Elkin, D. Tang, J. Meng, Mater. Sci. Eng. A 505 (2009) 13.